J. Fluid Mech. (1996), *vol.* 317, *pp.* 111–127

On finite-amplitude patterns of convection in a rectangular-planform container

By P. G. DANIELS[1] AND M. WEINSTEIN[2]

[1] Department of Mathematics, City University, Northampton Square, London EC1V 0HB, UK

[2] Raphael, PO Box 2250, Haifa 31021, Israel

(Received 15 February 1995 and in revised form 11 September 1995)

This paper considers the development of finite-amplitude patterns of convection in rectangular-planform containers. The horizontal dimensions of the container are assumed to be large compared with the critical wavelength of the motion. An interaction between rolls parallel and perpendicular to the lateral boundaries is modelled by a coupled pair of nonlinear amplitude equations together with appropriate conditions on the four lateral boundaries. At Rayleigh numbers above a critical value a steady-state solution is established with rolls parallel to the shorter lateral sides, consistent with the predictions of linear theory. At a second critical value this solution becomes unstable to cross-rolls near the shorter sides and a new steady state evolves. This consists of the primary roll pattern together with regions near the shorter sides where there is a combination of rolls parallel and perpendicular to the boundary.

Analytical and numerical methods are used to describe both the evolution and steady-state structure of the solution, and a comparison is made with the results of full numerical simulations and experiments.

1. Introduction

Convective patterns in fluid layers heated from below have been the subject of many theoretical, numerical and experimental studies. In a shallow container of rectangular planform it is known from linear theory that the main roll pattern at the onset of convection aligns with axes parallel to the shorter lateral sides of the container (Davis 1967). Weakly nonlinear effects were first incorporated using a multiple-scale approach by Newell & Whitehead (1969) and Segel (1969), and later Brown & Stewartson (1977) discussed the correct form of the boundary conditions for rolls parallel and perpendicular to the lateral walls. In any shallow container of rectangular planform with perfectly insulated walls, it appears that at sufficiently high Rayleigh numbers close to the onset of convection wholly two-dimensional solutions will not be realized in practice even in the region of flow distant from the lateral walls perpendicular to the primary roll pattern. The reason for this is that the region of reduced amplitude close to the lateral walls aligned parallel to the primary roll pattern becomes susceptible to an instability in the form of cross-rolls first analysed by Schluter, Lortz & Busse (1965) and in the context of the multiple-scale approach by Newell & Whitehead (1969). Such rolls require less space to adjust to the sidewall boundary conditions and therefore fill the low-amplitude zone of the two-dimensional solution.

Experimental observations described by Koschmieder (1993) and numerical simulations based on a model equation have confirmed the appearance of cross-rolls perpendicular to the primary roll pattern along the shorter lateral sides of a rectangular container. These rolls can be expected to affect the wavelength of the main roll pattern

predicted by a purely two-dimensional theory (Cross *et al.* 1983) and the local three-dimensional motion was therefore examined in detail by Daniels & Weinstein (1992). They found that in the steady state this three-dimensional motion consists of a nonlinear combination of rolls parallel and perpendicular to the boundary, with the latter confined to a region inside a critical transition line whose position depends on the precise nature of the boundary condition applied at the wall. This theory was based on an isolated infinitely long wall in which the roll pattern is not modulated along the length of the wall. For the case where the motion is fully confined to a rectangular domain by four lateral walls, modulation effects along the walls cannot be ignored. The present paper considers this situation and aims to describe the nonlinear steady-state structure that emerges in the slightly supercritical regime.

The analysis is based on a model equation introduced by Swift & Hohenberg (1977) for which numerical simulations have been carried out by Greenside & Coughran (1984). In §2 the overall amplitude equations governing weakly nonlinear solutions are set out and are then reduced to a coupled pair of second-order partial differential equations for the amplitudes of rolls parallel and perpendicular to the lateral boundaries in the main bulk of the rectangular container. Boundary conditions for these equations are obtained in the manner described by Daniels (1977) and Brown & Stewartson (1977). For a certain Prandtl number the same set of equations and boundary conditions also governs Rayleigh–Bénard convection between rigid horizontal boundaries and modifications for other Prandtl numbers do not alter the properties of the solution in a qualitative way. Thus the results presented here are also directly applicable to the physically realistic case of a fluid layer heated from below.

Analytical properties of the system are considered in §§3–5, focusing on the case where null conditions are applied at the lateral boundaries, equivalent to perfectly insulated or perfectly conducting walls in the Rayleigh–Bénard problem. Results are obtained which confirm the initial onset of rolls parallel to the shorter lateral boundaries and then, at a second critical point, the development of perpendicular rolls near these boundaries. The structure of the steady-state solution just beyond the second critical point is analysed in §4 using the method of matched asymptotic expansions. This analysis reveals that the perpendicular rolls are confined to a region close to the wall but that the amplitude of the main roll pattern is influenced significantly throughout the rectangular domain. Beyond the second critical point, a steady-state solution structure is envisaged consisting of the primary roll pattern together with regions of finite extent near the shorter sides where cross-rolls are present. This structure and the manner in which the transition lines which delineate the internal boundaries evolve at large times are described in §5. Confirmation of the structure is provided by full numerical solutions of the system, which are obtained using an explicit finite difference scheme and are described in §6. A detailed comparison is also made with the analytical predictions of §4. The results are discussed in relation to experimental work and the numerical simulations of Greenside & Coughran (1984) in §7.

2. Formulation

The model equation previously studied by Pomeau & Manneville (1980) is

$$\frac{\partial \psi}{\partial t} = (\epsilon - (\nabla^2 + 1)^2)\,\psi - \psi^3, \tag{2.1}$$

where ψ is a function of x, y and t, $\nabla^2 = \partial^2/\partial x^2 + \partial^2/\partial y^2$, x and y denote Cartesian

coordinates and t denotes time. This equation contains the essential ingredients of diffusion and cubic nonlinearity which characterize the Oberbeck–Boussinesq system and ϵ is a parameter equivalent to the excess of the Rayleigh number above its critical value for an infinite layer. Here a finite domain $0 \leqslant x \leqslant L$, $0 \leqslant y \leqslant M$ is assumed where both L and M are large compared with unity and on the lateral boundaries

$$\psi = \frac{\partial \psi}{\partial x} = 0 \quad (x = 0, L), \tag{2.2}$$

$$\psi = \frac{\partial \psi}{\partial y} = 0 \quad (y = 0, M), \tag{2.3}$$

conditions which imitate those associated with rigid impermeable walls.

The linearized form of equation (2.1) admits spatially periodic solutions when ϵ is greater than zero and the weakly nonlinear development of such solutions can be considered by writing

$$\psi \sim \{\mathscr{A} e^{ix} + \mathscr{B} e^{iy}\} + \text{c.c.}, \tag{2.4}$$

where $\mathscr{A}$ and $\mathscr{B}$ are complex, slowly varying functions of x, y and t, and c.c. denotes complex conjugate. The functions $\mathscr{A}$ and $\mathscr{B}$ represent the amplitudes of x-rolls and y-rolls (perpendicular and parallel to the x-direction respectively) and, provided these amplitudes are small, they satisfy as a first approximation, the equations

$$\frac{\partial \mathscr{A}}{\partial t} = \epsilon \mathscr{A} - 3\mathscr{A}(|\mathscr{A}|^2 + 2|\mathscr{B}|^2) + 4\left(\frac{\partial}{\partial x} - \frac{i}{2}\frac{\partial^2}{\partial y^2}\right)^2 \mathscr{A}, \tag{2.5}$$

$$\frac{\partial \mathscr{B}}{\partial t} = \epsilon \mathscr{B} - 3\mathscr{B}(|\mathscr{B}|^2 + 2|\mathscr{A}|^2) + 4\left(\frac{\partial}{\partial y} - \frac{i}{2}\frac{\partial^2}{\partial x^2}\right)^2 \mathscr{B}, \tag{2.6}$$

given by Daniels & Weinstein (1992).

These equations contain all possible leading-order variations with x, y and t and can be used as a basis for discussing the evolution of the system on lengthscales of order L and a timescale of order L^2. It is convenient to set

$$x = LX, \quad y = LY, \quad t = \tfrac{1}{4}L^2\tau \tag{2.7}$$

and

$$\mathscr{A} = \frac{2}{\sqrt{3}} L^{-1} A(X, Y, \tau), \quad \mathscr{B} = \frac{2}{\sqrt{3}} L^{-1} B(X, Y, \tau), \tag{2.8}$$

in which case for the regime where

$$\delta = \tfrac{1}{4}\epsilon L^2 \tag{2.9}$$

is finite, it follows from (2.5) and (2.6) that the system is governed to leading order by the coupled pair of amplitude equations

$$\frac{\partial A}{\partial \tau} = \frac{\partial^2 A}{\partial X^2} + \delta A - A(|A|^2 + 2|B|^2), \tag{2.10}$$

$$\frac{\partial B}{\partial \tau} = \frac{\partial^2 B}{\partial Y^2} + \delta B - B(|B|^2 + 2|A|^2). \tag{2.11}$$

Here finite values of δ are equivalent to an order-L^{-2} band of values of ϵ above the critical value for an infinite layer, $\epsilon = 0$. It is important to recognize that although the scalings (2.7) lead to the absence of Y- and X-derivatives in (2.10) and (2.11) respectively, both A and B will in general vary with both X and Y through the nonlinear interaction.

Boundary conditions for the system (2.10), (2.11) can be derived by considering a linearized version of (2.1) in the manner described by Daniels & Weinstein (1992), leading to the requirement that

$$A = 0 \quad \text{at} \quad X = 0 \quad \text{and} \quad X = 1, \tag{2.12}$$

and similarly

$$B = 0 \quad \text{at} \quad Y = 0 \quad \text{and} \quad Y = a, \tag{2.13}$$

where $a = M/L$ is the aspect ratio of the rectangular planform. The absence of conditions on B at $X = 0$, 1 and A at $Y = 0$, a is consistent with the form of equations (2.10), (2.11). A necessary adjustment to the amplitude of rolls perpendicular to the boundaries in order to accommodate the full boundary conditions (2.2), (2.3) occurs primarily within boundary layers of thickness $x \sim L^{1/2}$ and $y \sim L^{1/2}$ where the fourth-order spatial derivatives in (2.5) and (2.6) come into play. These boundary layers are discussed by Brown & Stewartson (1977) and Daniels & Weinstein (1992) and are generally passive, allowing the amplitude and gradient in amplitude of rolls perpendicular to the boundary to reduce to zero at the boundary. Thus in the context of the full amplitude equations (2.5), (2.6), a solution would have to be found subject to the additional conditions $\mathscr{A} = \partial\mathscr{A}/\partial y = 0$ at $y = 0, M$ and $\mathscr{B} = \partial\mathscr{B}/\partial x = 0$ at $x = 0, L$, whereas the reduced system (2.10)–(2.13) is free of this added complication.

The system (2.10)–(2.13) also governs Rayleigh–Bénard convection in a rectangular container with rigid horizontal boundaries and either perfectly insulating or perfectly conducting lateral walls. In this case, δ is equivalent to an order-L^{-2} band of values of the Rayleigh number above the critical value for an infinite layer and each of the coefficients of 2 in the equations (2.10) and (2.11) is replaced by a Prandtl-number-dependent coefficient whose value varies from 1.23 for infinite Prandtl number to 14.3 for a Prandtl number of zero. For this range of values there is likely to be no qualitative difference in the behaviour of solutions as compared with those of (2.10)–(2.13). A full derivation of the equivalent Rayleigh–Bénard system based on results obtained previously by, for example, Schluter *et al.* (1965), Cross (1980) and Daniels & Ong (1990) is given by Sivapragasam (1995).

Daniels & Weinstein (1992) considered an infinitely long isolated wall at $X = 0$, allowing the parameter δ to be scaled out of the equations (2.10), (2.11) and solutions for A and B to be found independent of Y in the semi-infinite domain $X \geqslant 0$ subject to $A = \lambda$ at $X = 0$ (including the case $\lambda = 0$) and $A \to \delta^{1/2}$ as $X \to \infty$. Such solutions cannot be valid for the finite rectangular domain where the boundary conditions (2.12), (2.13) apply, although they may relate to the limiting form of the solution in the finite domain as $\delta \to \infty$ in a manner to be discussed further in §7. In particular it is clear that if B is non-zero, (2.12), (2.13) and (2.10) imply that both B and A must depend on Y, an essential feature of this investigation not present in the analysis of Daniels & Weinstein (1992).

3. Onset of convection

One steady-state solution of (2.10)–(2.13) is $A = B = 0$ but this state of no motion becomes unstable when δ exceeds a critical value and convective rolls then develop. There are clearly steady-state solutions for which only one set of rolls is present. For example, with $B = 0$, solutions of equation (2.10) subject to (2.12) appear as bifurcations at $\delta = n^2\pi^2$ ($n = 1, 2, \ldots$). The leading branch of solutions is given by

$$A = \mathrm{e}^{\mathrm{i}\alpha}\left(\frac{2\delta m}{m+1}\right)^{1/2} \mathrm{sn}\,(U, m), \quad \delta > \pi^2, \tag{3.1}$$

where $U = (\delta/(m+1))^{1/2}X$ and m is determined from the boundary conditions by the relation

$$\delta^{1/2} = 2(1+m)^{1/2}K(m). \tag{3.2}$$

Here sn is the Jacobian elliptic function and K is the complete elliptic integral of the first kind (see for example Abramowitz & Stegun 1965, p. 569). This set of solutions bifurcates from the zero solution at $\delta = \pi^2$ and except near $X = 0$ and $X = 1$ approaches the uniform profile $|A| \sim \delta^{1/2}$ as $\delta \to \infty$, equivalent to rolls of constant amplitude filling most of the container. Solutions of this type are discussed by Segel (1969) and Daniels (1977). Higher branches correspond to taking integer multiples of the right-hand side of (3.2) but are likely to represent unstable flow patterns. The real parameter α, which may depend on Y, is arbitrary as far as the steady-state system is concerned. Physically, this is equivalent to a lack of knowledge of the precise lateral position of individual rolls in the container. In practice for the full system (2.1)–(2.3) the phase of the solution in the final steady state is determined by higher-order effects in the expansion in inverse powers of L on a timescale $t = O(L^3)$, longer than that encompassed by (2.10)–(2.13), and in the manner explained by Daniels (1978). Within the context of the present system (2.10)–(2.13) the form of $\alpha(Y)$ will be determined by whatever initial conditions are specified at $\tau = 0$. Thus, for example, if A and B are specified as real initially then they will remain so for all $\tau > 0$.

In a similar way, steady-state solutions of (2.10)–(2.13) for B remain arbitrary to within a multiplicative factor $e^{i\beta}$, where β may depend on X. With $A = 0$, solutions for B emerge as bifurcations at $\delta = n^2\pi^2/a^2$ ($n = 1, 2, \ldots$) and can also be expressed in terms of Jacobian elliptic functions. Clearly if $a < 1$, x-rolls appear ahead of y-rolls, consistent with the well-known result obtained numerically by Davis (1967) and experimentally by Chen & Whitehead (1968) that, in large-planform rectangular systems, convection occurs first in the form of rolls parallel to the shorter sides of the container.

It is worth noting that solutions such as (3.1), (3.2) are also applicable generally on the boundaries $Y = 0$ and $Y = a$ because B always vanishes there (by (2.13)) even when it is non-zero elsewhere in the domain. Similarly, solutions for B can be written down analytically on the boundaries $X = 0$ and $X = 1$.

4. Emergence of orthogonal rolls near the lateral boundaries

Consider the case where the aspect ratio $a < 1$. As δ is increased above the value π^2, the steady-state motion in the main body of the container will consist of x-rolls whose amplitude is independent of y but varies with x across the width of the container, as given by (3.1). However, this finite-amplitude solution will itself become unstable to y-rolls in regions where the amplitude of x-rolls is sufficiently low, as pointed out by Pomeau & Zaleski (1981). In the present system this can be seen by considering a small perturbation to the steady-state solution $|A| = R(X)$ given by (3.1) which allows for a cross-roll disturbance of the form

$$B = B_0(X, Y)\, e^{\sigma(X)\tau}, \quad B_0 \ll 1. \tag{4.1}$$

Then it is readily shown from (2.11) and (2.13) that the highest growth rate corresponds to an eigenfunction

$$B_0 = \tilde{B}_0(X) \sin(\pi Y/a), \tag{4.2}$$

with

$$\sigma = \delta - \frac{\pi^2}{a^2} - 2R^2(X). \tag{4.3}$$

Thus the solution (3.1) is unstable to y-rolls in any region where its amplitude R is less than $\{(\delta-\pi^2/a^2)/2\}^{1/2}$. Since R vanishes at the lateral walls $x=0$ and $x=L$, y-rolls can be expected to develop there when δ exceeds the critical value π^2/a^2 and then to spread inwards as δ increases. This process is counterbalanced by the increase in amplitude of the x-roll pattern with δ and it is interesting to conjecture what steady-state structure the solution will adopt at general values of δ greater than π^2/a^2. The following analysis for values of δ slightly greater than π^2/a^2 provides insight into this structure.

In view of the results (3.1) and (4.3) it is expected that as $\delta \to \pi^2/a^2+$, the domain subdivides into an outer region $0<X<1$, $0 \leqslant Y \leqslant a$, an inner region near the boundary $x=0$ where $0 \leqslant Y \leqslant a$ and X is of order $(\delta-\pi^2/a^2)^{1/2}$, and a similar inner region near the boundary $x=L$. It is convenient to introduce a small parameter

$$\bar{\delta} = \delta - \frac{\pi^2}{a^2} \tag{4.4}$$

and in the outer region the solution for B is zero (to algebraic orders in $\bar{\delta}$) while

$$A = e^{i\alpha}\{A_0(X,Y)+\bar{\delta}A_1(X,Y)+\bar{\delta}^2A_2(X,Y)+\bar{\delta}^{5/2}A_3(X,Y)+\ldots\}, \quad \bar{\delta}\to 0, \tag{4.5}$$

where α is an arbitrary real function of Y and A_i are real functions of X and Y. Successive terms are generated either by nonlinear effects, $\bar{\delta}$ itself or the inner solution to be discussed below. The leading-order approximation A_0 satisfies

$$\frac{\partial^2 A_0}{\partial X^2}+\frac{\pi^2}{a^2}A_0-A_0^3=0, \tag{4.6}$$

with boundary conditions $A_0=0$ at $X=0$ and $X=1$, and the relevant solution is given by (3.1) and (3.2) with δ replaced by π^2/a^2, namely

$$A_0 = \left(\frac{2m}{m+1}\right)^{1/2}\frac{\pi}{a}\,\mathrm{sn}\,(U,m), \quad U=\pi X/(1+m)^{1/2}a, \tag{4.7}$$

where

$$\pi/a = 2(1+m)^{1/2}K(m). \tag{4.8}$$

As $X\to 0$, this solution has the form

$$A_0 = \mu_1 X+\mu_3 X^3+\mu_5 X^5+\ldots, \tag{4.9}$$

where

$$\mu_1 = 4(2m)^{1/2}K^2(m), \quad \mu_3 = -\pi^2\mu_1/6a^2, \quad \mu_5 = (\mu_1^3-\pi^2\mu_3/a^2)/20. \tag{4.10}$$

Further terms A_i $(i=1,2,\ldots)$ satisfy

$$\frac{\partial^2 A_i}{\partial X^2}+\frac{\pi^2}{a^2}A_i-3A_0^2A_i=\chi_i, \tag{4.11}$$

where $\chi_1=-A_0$, $\chi_2=3A_0A_1^2-A_1$ and $\chi_3=0$. The solutions for A_1 and A_2 must vanish at $X=0$ and $X=1$ but A_3 is non-zero there and the relevant boundary conditions are obtained by consideration of the inner region.

In the inner region near $x=0$, the solution is expressed in terms of a local coordinate $\bar{X}$ defined by

$$\bar{X} = \bar{\delta}^{-1/2}X, \tag{4.12}$$

with

$$A = e^{i\alpha}\{\bar{\delta}^{1/2}\bar{A}_0+\bar{\delta}^{3/2}\bar{A}_1+\bar{\delta}^{5/2}\bar{A}_2+\ldots\}, \tag{4.13}$$

$$B = e^{i\beta}\{\bar{\delta}^{1/2}\bar{B}_0+\bar{\delta}^{3/2}\bar{B}_1+\bar{\delta}^{5/2}\bar{B}_2+\ldots\}, \tag{4.14}$$

where β is an arbitrary function of $\bar{X}$ and $\bar{A}_0$, $\bar{B}_0$, ... are real functions of $\bar{X}$ and Y. Substitution into (2.9) shows that $\bar{A}_0$ is a linear function of $\bar{X}$ and the only solution which vanishes at $\bar{X}=0$ and matches with (4.5) as $\bar{X}\to\infty$ is

$$\bar{A}_0 = \mu_1 \bar{X}. \tag{4.15}$$

From (2.11), $\bar{B}_0$ must satisfy

$$\frac{\partial^2 \bar{B}_0}{\partial Y^2}+\frac{\pi^2}{a^2}\bar{B}_0 = 0, \quad \bar{B}_0 = 0 \quad (Y=0,a), \tag{4.16}$$

giving

$$\bar{B}_0 = b_0(\bar{X})\sin(\pi Y/a), \tag{4.17}$$

where b_0 is a function of $\bar{X}$ to be determined.

In (2.10), terms of order $\bar{\delta}^{1/2}$, together with the boundary condition at $\bar{X}=0$, give

$$\bar{A}_1 = \mu_3 \bar{X}^3+\nu_1 \bar{X}, \tag{4.18}$$

where $\nu_1 = \partial A_1/\partial X(0, Y)$. In (2.11), terms of order $\bar{\delta}^{3/2}$ give

$$\frac{\partial^2 \bar{B}_1}{\partial Y^2}+\frac{\pi^2}{a^2}\bar{B}_1 = \bar{B}_0(\bar{B}_0^2+2\bar{A}_0^2-1), \quad \bar{B}_1 = 0 \quad (Y=0,a). \tag{4.19}$$

This system has a solution only if

$$\int_0^a \bar{B}_0^2(\bar{B}_0^2+2\bar{A}_0^2-1)\,\mathrm{d}Y = 0, \tag{4.20}$$

which gives either $b_0 = 0$ or

$$b_0 = 2(1-2\mu_1^2\bar{X}^2)^{1/2}/\sqrt{3}, \quad \bar{X}<\bar{X}_0, \tag{4.21}$$

where $\bar{X}_0 = 1/\sqrt{2}\mu_1$. The only feasible solution for $\bar{X}>\bar{X}_0$ is $b_0=0$ and from the earlier discussion it is envisaged that for $\bar{X}<\bar{X}_0$, the solution (4.21) represents the stable steady-state form. Thus in the region near the wall, $0<\bar{X}<\bar{X}_0$, x- and y-rolls of comparable amplitude coexist, while outside the transition line $\bar{X}=\bar{X}_0$ only x-rolls are present. The nature of the abrupt change in amplitude of y-rolls in the neighbourhood of the transition line is discussed in detail in §5.

In (2.10), terms of order $\bar{\delta}^{3/2}$ give

$$\frac{\partial^2 \bar{A}_2}{\partial \bar{X}^2} = \bar{A}_0(\bar{A}_0^2+2\bar{B}_0^2-1)-\frac{\pi^2}{a^2}\bar{A}_1, \tag{4.22}$$

which shows that the solution for $\bar{A}_2$ is influenced by the presence of the y-rolls. This equation must be integrated separately on each side of the transition line and this gives

$$\bar{A}_2 = \mu_5\bar{X}^5-\frac{1}{6}\left(\mu_1+\frac{\nu_1\pi^2}{a^2}\right)\bar{X}^3+\tfrac{4}{3}\mu_1(\tfrac{1}{3}\bar{X}^3-\tfrac{1}{5}\mu_1^2\bar{X}^5)\sin^2(\pi Y/a)+\bar{\omega}_1\bar{X}, \quad \bar{X}<\bar{X}_0, \tag{4.23}$$

having made use of the fact that $\bar{A}_2=0$ at $\bar{X}=0$, and

$$\bar{A}_2 = \mu_5\bar{X}^5-\frac{1}{6}\left(\mu_1+\frac{\nu_1\pi^2}{a^2}\right)\bar{X}^3+\omega_1\bar{X}+\omega, \quad \bar{X}>\bar{X}_0, \tag{4.24}$$

where ω is an arbitrary function of Y and from matching with the outer solution, $\omega_1 = \partial A_2/\partial X(0, Y)$. Continuity of $\bar{A}_2$ and $\partial\bar{A}_2/\partial\bar{X}$ at $\bar{X}=\bar{X}_0$ now gives

$$\bar{\omega}_1 = \omega_1-\tfrac{1}{3}\mu_1^{-1}\sin^2(\pi Y/a) \tag{4.25}$$

and

$$\omega = -\frac{4\sqrt{2}}{45\mu_1^2}\sin^2(\pi Y/a). \tag{4.26}$$

The solution for $\bar{A}_2$ is of particular interest because it shows how the amplitude of the x-rolls varies with Y throughout the inner region and that this variation extends, via the solution for ω above, into the region outside the transition line. This variation in turn influences the outer solution through the matching condition

$$A_3(0, Y) = \omega, \tag{4.27}$$

which provides one boundary condition for the outer function A_3. By symmetry, the other boundary condition is

$$A_3(1, Y) = \omega \tag{4.28}$$

and it follows that there is an order-$\bar{\delta}^{5/2}$ variation with Y in the amplitude of the main x-roll pattern throughout the container, associated with the outer term $A_3(X, Y)$.

The general solution for A_3 can be expressed in the form

$$A_3 = c_1\frac{\partial \mathrm{sn}}{\partial U}(U,m)+c_2\left\{\mathrm{sn}\,(U,m)+2m(1+m)\frac{\partial \mathrm{sn}}{\partial m}(U,m)-mU\frac{\partial \mathrm{sn}}{\partial U}(U,m)\right\}, \tag{4.29}$$

but only the even part of the solution is generated by the conditions (4.27) and (4.28), giving $c_1 = \omega$ and

$$c_2 = \frac{\omega}{m\{2(1+m)\,\mathrm{d}K/\mathrm{d}m + K(m)\}}. \tag{4.30}$$

Solutions for A_1 and A_2 can also be expressed in terms of Jacobian elliptic functions but are independent of Y and are just equivalent to the order-$\bar{\delta}$ and order-$\bar{\delta}^2$ terms obtained by expanding the solution given by (3.1) and (3.2) about the point $\delta = \pi^2/a^2$. Thus the above results show that across the centre of the container, $x = \frac{1}{2}L$, the x-roll amplitude can be approximated by

$$|A| = \left(\frac{2\delta m}{1+m}\right)^{1/2} - \frac{\sqrt{2}\,(\delta-\pi^2/a^2)^{5/2}\sin^2(\pi Y/a)}{360m^2\{2(1+m)\,\mathrm{d}K/\mathrm{d}m + K(m)\}\{K(m)\}^4} \tag{4.31}$$

as $\delta \to \pi^2/a^2+$. The deficit in amplitude of a given x-roll at its mid-point, $Y = \frac{1}{2}a$, compared with its maximum amplitude near each lateral wall, $Y = 0, a$, changes from a value of

$$D_0 \sim \frac{\sqrt{2}}{360m\{K(m)\}^4}(\delta-\pi^2/a^2)^{5/2} \tag{4.32}$$

near the boundaries $x = 0$ and $x = L$ to the value

$$D_{1/2} \sim \frac{\sqrt{2}}{360m^2\{2(1+m)\,\mathrm{d}K/\mathrm{d}m + K(m)\}\{K(m)\}^4}(\delta-\pi^2/a^2)^{5/2} \tag{4.33}$$

given by (4.31) at $x = \frac{1}{2}L$. The variation of the main properties of the solution with the aspect ratio a is shown in table 1.

The analysis can be extended to obtain further properties of the solution. For example, $\bar{B}_1$ can be obtained as

$$\bar{B}_1 = b_1(\bar{X})\sin(\pi Y/a) + \frac{a^2b_0^3}{32\pi^2}\sin(3\pi Y/a), \tag{4.34}$$

m	a	μ_1	$\bar{X}_0$	$A_0(X=\frac{1}{2})$	$\bar{\delta}^{-5/2}D_0$	$\bar{\delta}^{-5/2}D_{1/2}$
0	1	0	∞	0	∞	∞
0.1	0.929	4.651	0.152	1.442	0.00581	0.02248
0.2	0.864	6.968	0.101	2.099	0.00259	0.00451
0.3	0.804	9.101	0.077	2.655	0.00152	0.00156
0.4	0.747	11.304	0.063	3.180	0.00098	0.00066
0.5	0.692	13.750	0.051	3.708	0.00067	0.00030
0.6	0.637	16.654	0.042	4.271	0.00045	0.00014
0.7	0.581	20.385	0.035	4.911	0.00030	0.00006
0.8	0.519	25.779	0.027	5.710	0.00019	0.00002
0.9	0.442	35.669	0.020	6.918	0.00010	0.00001
1.0	0	∞	0	∞	0	0

TABLE 1. Properties of the small-$\bar{\delta}$ solution for various aspect ratios in the range $0 \leqslant a \leqslant 1$

where solvability of the equation for $\bar{B}_2$ leads to the requirement that

$$b_1 = \frac{a^2 b_0^3}{64\pi^2} - \frac{8\mu_1 \bar{X}^2(\mu_3 \bar{X}^2 + \nu_1)}{3b_0}. \tag{4.35}$$

This in turn leads to a correction to the location of the transition line where B falls to zero so that from (4.21) and (4.35),

$$B \sim e^{i\beta} \frac{2^{7/4}}{\sqrt{3}} \mu_1^{1/2} \bar{\delta}^{1/2} (\bar{X}_T - \bar{X})^{1/2} \sin(\pi Y/a), \quad \bar{X} \to \bar{X}_T -, \tag{4.36}$$

where $\bar{X}_T = \bar{X}_0 + \bar{\delta}\bar{X}_1 + \ldots$ $(\bar{\delta} \to 0)$ defines the location of the transition line and

$$\bar{X}_1 = -2^{-3/2} \mu_1^{-4} (\mu_3 + 2\nu_1 \mu_1^2). \tag{4.37}$$

In crystal growth terminology this transition line is known as a grain boundary and its location and dynamics are of some significance. The emergence of a steady-state structure with stationary transition lines near each of the shorter lateral boundaries is in contrast to the result for the semi-infinite problem studied by Daniels & Weinstein (1992) where, with $A = 0$ on $X = 0$, the transition line continues to move slowly away from the wall at large times. Further discussion of this point is given in §7.

5. General steady-state structure and evolution of the transition lines

The results of §4 suggest a stable steady-state configuration for $\delta > \pi^2/a^2$ in which, for a container of aspect ratio $a < 1$, both x-rolls and y-rolls coexist, with the y-rolls limited to regions within transition lines $X = X_T$ and $X = 1 - X_T$ near each of the lateral boundaries $x = 0$ and $x = L$. Near each transition line the amplitude of the y-roll pattern falls rapidly, leading to a discontinuity in the gradient of B. Confirmation that this is an acceptable steady-state configuration would require consideration of a local structure near the transition line where it can be expected that the second-order derivative of $\mathscr{B}$ with respect to x which appears in (2.6) plays a significant role on a lengthscale in X of order $L^{-1/3}$. In the present paper, attention is focused on the properties of (2.10)–(2.13) and it is possible to describe the way in which the local structure evolves near X_T by considering the form of the solution as $\tau \to \infty$.

At general values of $\delta > \pi^2/a^2$ a steady-state structure is envisaged in which the central zone $X_T < X < 1 - X_T$ contains a solution of (2.10) in which $B = 0$ and A is a

function of both X and Y. The dependence on Y is due to the requirement that A and $\partial A/\partial X$ are continuous at the transition lines $X = X_T$, $1-X_T$. The solutions in $X < X_T$ and $X > 1-X_T$ must satisfy the full steady-state versions of (2.10), (2.11) with both A and B dependent on X and Y, and B approaching zero as $X \to X_T-$ and $X \to (1-X_T)+$. Unlike the Y-independent situation studied by Daniels & Weinstein (1992) the nonlinear problems in these side zones cannot be solved analytically. However, it is possible to consider the manner in which the steady-state solution is achieved as $\tau \to \infty$ in the neighbourhood of the transition lines, generalizing the analysis of Daniels & Weinstein (1992) to the case where the roll amplitudes are dependent on Y.

Consider the transition line at $X = X_T$ and assume that locally

$$A = \mathrm{e}^{\mathrm{i}\alpha}\{\tilde{A}_0(Y) + (X-X_T)\,\tilde{A}_1(Y) + \ldots\}, \quad X \to X_T, \tag{5.1}$$

where the precise forms of the real functions $\tilde{A}_0$ and $\tilde{A}_1$ are determined by the outer problems described above. As $\tau \to \infty$, a solution for B near X_T is sought in the form

$$B = \mathrm{e}^{\mathrm{i}\beta}\{\tau^{-1/2}\,\tilde{B}_0(\eta, Y) + \tau^{-3/2}\,\tilde{B}_1(\eta, Y) + \ldots\}, \tag{5.2}$$

where $\eta = (X-X_T)\tau$. Then substitution into (2.11) shows that at leading order $\tilde{B}_0$ satisfies

$$\frac{\partial^2 \tilde{B}_0}{\partial Y^2} + \delta \tilde{B}_0 - 2\tilde{A}_0^2\,\tilde{B}_0 = 0, \quad \tilde{B}_0 = 0 \quad (Y = 0, a) \tag{5.3}$$

and at second order

$$\left.\begin{aligned} \frac{\partial^2 \tilde{B}_1}{\partial Y^2} + \delta \tilde{B}_1 - 2\tilde{A}_0^2\,\tilde{B}_1 = \eta \frac{\partial \tilde{B}_0}{\partial \eta} - \tfrac{1}{2}\tilde{B}_0 + \tilde{B}_0^3 + 4\eta \tilde{A}_0\,\tilde{A}_1\,\tilde{B}_0, \\ \tilde{B}_1 = 0 \quad (Y = 0, a). \end{aligned}\right\} \tag{5.4}$$

The definition of η and the chosen magnitude of B ensure that effects of both nonlinearity and spatial variation contribute on the right-hand side of (5.4). From (5.3) the solution for $\tilde{B}_0$ can be written in the form

$$\tilde{B}_0 = \tilde{B}(\eta)\,F(Y), \tag{5.5}$$

where

$$F'' + \delta F - 2\tilde{A}_0^2 F = 0, \quad F = 0 \quad (Y = 0, a). \tag{5.6}$$

The existence of a solution of this eigenvalue problem effectively defines the location of the transition line $X = X_T$. Multiplication of (5.3) and (5.4) by $\tilde{B}_1$ and $\tilde{B}_0$ respectively, subtraction and integration from $Y = 0$ to $Y = a$ shows that the system (5.4) has a solution for $\tilde{B}_1$ only if

$$d_1\left(\eta \frac{\mathrm{d}\tilde{B}}{\mathrm{d}\eta} - \tfrac{1}{2}\tilde{B}\right) + d_2\,\tilde{B}^3 + 4d_3\,\eta \tilde{B} = 0, \tag{5.7}$$

where $d_i\,(i = 1, 2, 3)$ are positive constants defined by

$$d_1 = \int_0^a F^2\,\mathrm{d}Y, \quad d_2 = \int_0^a F^4\,\mathrm{d}Y, \quad d_3 = \int_0^a \tilde{A}_0\,\tilde{A}_1 F^2\,\mathrm{d}Y. \tag{5.8}$$

A solution of (5.7) is required for which

$$\tilde{B} \to 0 \quad \text{as} \quad \eta \to \infty \tag{5.9}$$

and for which

$$\tilde{B} \sim 2(-d_3\eta/d_2)^{1/2} \quad \text{as} \quad \eta \to -\infty. \tag{5.10}$$

These conditions are consistent with the requirement that B vanishes in the central zone $X_T < X < 1-X_T$ and attains a finite-amplitude form in the side zone $X < X_T$. The required solution which avoids a singularity at $\eta = 0$ and decays exponentially as $\eta \to \infty$ is

$$\tilde{B}(\eta) = (d_1/d_2)^{1/2}\,\hat{B}(\hat{\eta}), \tag{5.11}$$

where

$$\hat{B}(\hat{\eta}) = 2\left(\frac{\hat{\eta}}{e^{8\hat{\eta}}-1}\right)^{1/2}, \quad \hat{\eta} = d_3\eta/d_1, \tag{5.12}$$

and this provides a smooth transition between the side zone and the central zone at large times. As $\tau \to \infty$, the width of the transition zone approaches zero ($X - X_T \sim \tau^{-1}$) and locally the amplitude of y-rolls is small (of order $\tau^{-1/2}$) with a form proportional to $(X_T - X)^{1/2}$ as $X \to X_T -$.

The above solution can be quantified in the case where δ is close to π^2/a^2 because it follows from §4 that

$$\tilde{A}_0 \approx (\bar{\delta}/2)^{1/2}, \quad \tilde{A}_1 \approx \mu_1 \tag{5.13}$$

and

$$F \approx \sin(\pi Y/a), \quad d_1 \approx \tfrac{1}{2}a, \quad d_2 \approx \tfrac{3}{8}a, \quad d_3 \approx (\bar{\delta}/8)^{1/2}\mu_1 a, \tag{5.14}$$

where $\bar{\delta} = \delta - \pi^2/a^2$. Thus

$$B \sim \frac{2}{\sqrt{3}} e^{i\beta}\tau^{-1/2}\,\hat{B}(\hat{\eta})\sin(\pi Y/a), \tag{5.15}$$

where

$$X = (\bar{\delta}/2)^{1/2}\mu_1^{-1} + (2/\bar{\delta})^{1/2}\mu_1^{-1}\tau^{-1}\hat{\eta}. \tag{5.16}$$

As $\tau \to \infty$ the transition region accommodates a smooth adjustment from the parabolic form (4.21) as $\hat{\eta} \to -\infty$ to an exponentially small form as $\hat{\eta} \to \infty$. As $\bar{\delta} \to 0$, the width of the transition zone, $X - X_T$, is of order $\bar{\delta}^{-1/2}\tau^{-1}$ which is small compared with the width of the side zone provided $\tau \gg \bar{\delta}^{-1} \gg 1$.

At general values of $\delta > \pi^2/a^2$ the results of this section show that the y-roll amplitude falls rapidly to zero within a lengthscale in X of order τ^{-1}, so that the adjustment occurs across a region which narrows as $\tau \to \infty$. This behaviour continues until the width of the transition zone is comparable with the scale of order $L^{-1/3}$ on which the derivatives in x come into play in (2.6) and at this stage a local steady-state configuration can be expected to emerge.

6. Numerical results

Some solutions of (2.10)–(2.13) were computed numerically from initial distributions of the form

$$A = \sin \pi X, \quad B = \sin(\pi Y/a) \quad \text{at} \quad \tau = 0. \tag{6.1}$$

The system was discretized onto a uniform grid in X and Y and an explicit scheme used to follow the evolution in time, using a time step $\Delta\tau$ satisfying the stability criterion for the corresponding linear diffusion equations. For most computations, step lengths $\Delta X = 0.02$ and $\Delta Y = 0.02$ were used, with $\Delta\tau = 0.0001$, and checks on accuracy were made using other values.

Figures 1–4 show results for an aspect ratio $a = 0.6$ and various values of δ. In

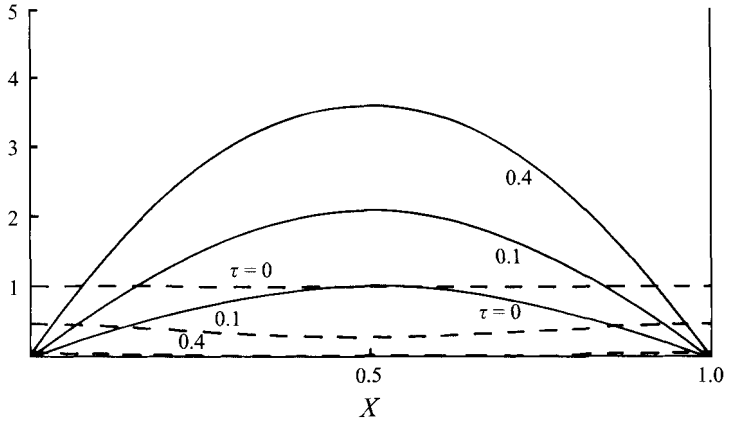

FIGURE 1. Profiles of A and B shown by solid and dashed lines respectively on the centreline $Y = 0.3$ at various times τ for $\delta = 20$ and an aspect ratio $a = 0.6$.

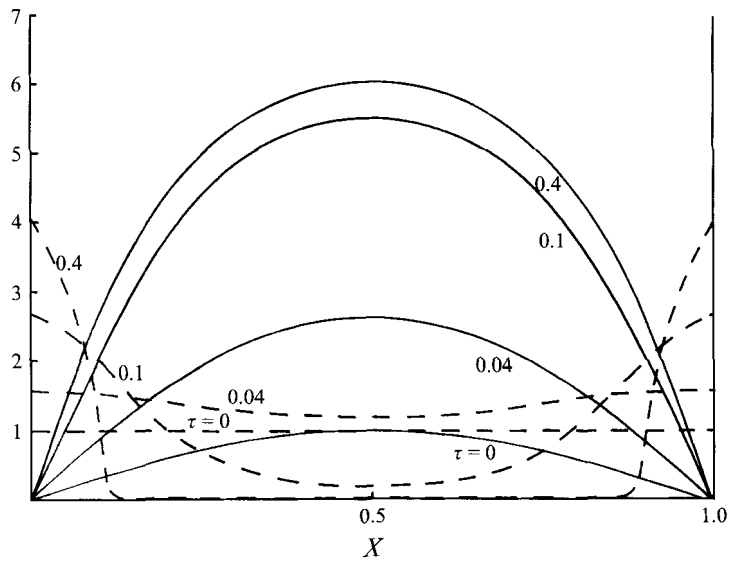

FIGURE 2. Profiles of A and B shown by solid and dashed lines respectively on the centreline $Y = 0.3$ at various times τ for $\delta = 40$ and an aspect ratio $a = 0.6$.

figure 1, the value $\delta = 20$ is above the critical value π^2 at which an x-roll pattern is expected to emerge but below the value $\pi^2/a^2 \approx 27.4$ at which y-rolls should persist near the lateral walls $X = 0$ and $X = 1$. The numerical computation confirms the growth of the x-roll amplitude, and the one-dimensional solution (3.1) evolves at sufficiently large times. In practice this steady state is achieved by the time τ reaches a value of about 0.4, and at this point the amplitude A is virtually independent of Y; the profile on the centreline, $Y = 0.3$, is shown in figure 1.

Figure 2 shows the solution for $\delta = 40$, at which point the critical value for the persistence of y-rolls near the lateral walls is exceeded. The numerical results confirm that the y-roll amplitude increases near $X = 0$ and $X = 1$, and decreases to zero in the central portion of the container, with transition lines centred near $X \approx 0.1$ and $X \approx 0.9$ as τ increases. Steepening transition zones surround these lines in the manner predicted by the analysis of §5 and elsewhere a steady state is again achieved by the time τ

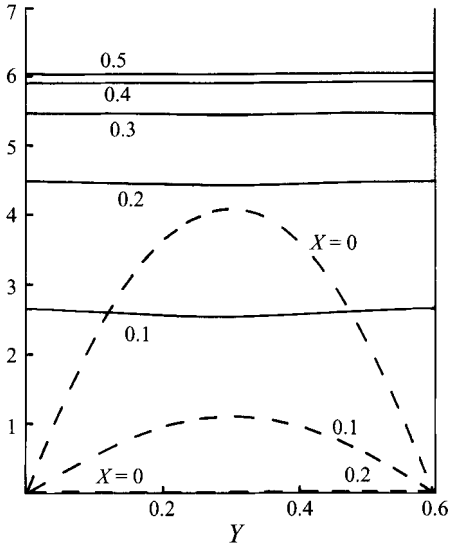

FIGURE 3. Profiles of A and B shown by solid and dashed lines respectively at various values of X when $\tau = 0.4$ for $\delta = 40$ and an aspect ratio $a = 0.6$.

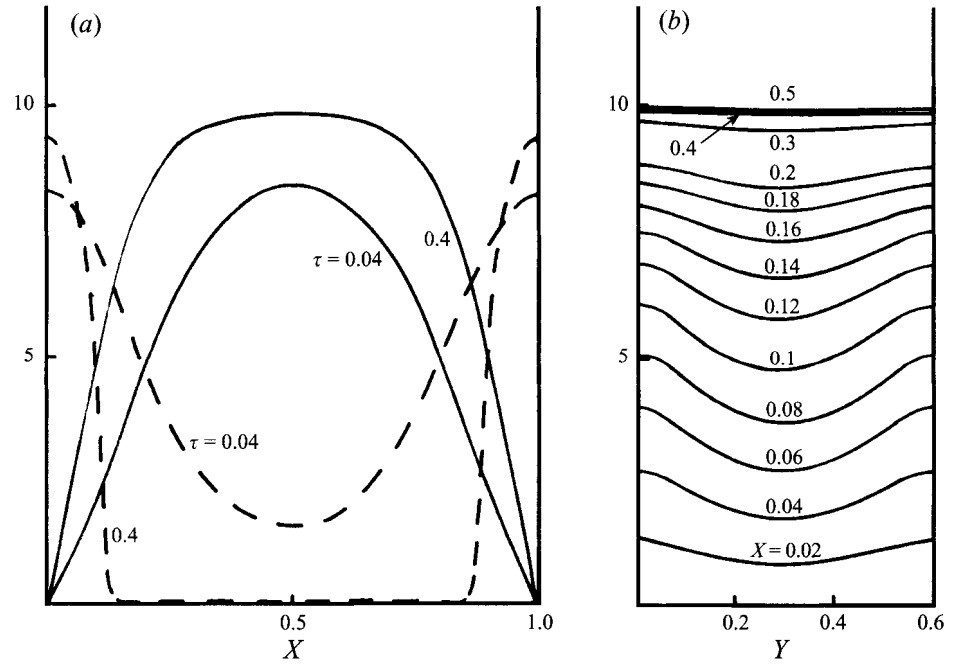

FIGURE 4. Results for $\delta = 100$ and an aspect ratio $a = 0.6$ giving (a) profiles of A and B shown by solid and dashed lines respectively on the centreline $Y = 0.3$ at various times τ and (b) profiles of A at various values of X when $\tau = 0.4$.

reaches a value of about 0.4. Figure 3 shows the dependence of the solution on Y, and unlike the previous case ($\delta = 20$), the solution for A remains dependent on Y throughout the container. This dependence is weak in the central region $0.1 < X < 0.9$, as expected from the analysis of §4.

Results for $\delta = 100$ shown in figure 4 display further evidence of the Y-dependence

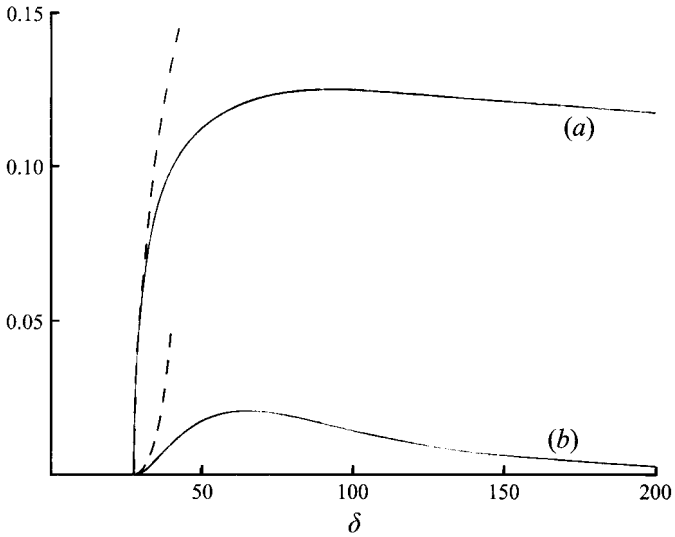

FIGURE 5. Variation for $a = 0.6$ of (a) the location of the transition line with δ, as measured by the value of X at which $A = (\delta - \pi^2/a^2)^{1/2}/\sqrt{2}$ on $Y = a/2$; the dashed line indicates the asymptote $X \sim \bar{\delta}^{1/2}/\sqrt{2\mu_1}$, $\bar{\delta} \to 0$ predicted by the analysis of §4, (b) the amplitude deficit $D_{1/2}$; the dashed line indicates the asymptote (4.33).

of the solution. This is again weaker near the centre, $X = 0.5$, but is quite significant near the transition line located at $X \approx 0.12$. At $\tau = 0.4$, the steady-state profile of A across the central portion of the container indicates the attainment of a plateau where $A \approx \delta^{1/2}$, corresponding to an x-roll pattern of constant amplitude throughout most of the container.

Figure 5 shows how the extent of the region of cross-rolls near $X = 0$ varies as a function of δ for the steady-state solution with $a = 0.6$. For convenience the value of X at which $A = (\delta - \pi^2/a^2)^{1/2}/\sqrt{2}$ on $Y = a/2$ is used as a measure of the location of the transition line, since this provides an approximation to the line along which B falls to zero, and is readily estimated from the numerical data. It is seen that the region expands rapidly just beyond the critical point $\delta \approx 27.4$ but then contracts again beyond $\delta \approx 100$, never occupying more than about 12% of the total area of the planform when $a = 0.6$. Also shown in figure 5 is the steady-state amplitude deficit

$$D_{1/2} = A|_{X=1/2,\, Y=0} - A|_{X=1/2,\, Y=a/2} \tag{6.2}$$

for $a = 0.6$, which reaches a maximum near $\delta = 65$ and then decreases to zero as $\delta \to \infty$. Figure 6 shows a detailed comparison of the computed location of the transition line and amplitude deficit near the critical point with the asymptotic results derived in §4. Here it was necessary to compute solutions up to $\tau = 3$ in order to achieve a reasonable steady state and the results indicate excellent agreement with the asymptotic analysis.

Numerical solutions were also obtained for other values of a. In particular, results were obtained for $a = 0.2$, 0.8, 0.9 and 0.96 which had the same qualitative features as those for $a = 0.6$. Detailed investigation of the solution for $a = 0.9$ just beyond the second critical point, $\delta = \pi^2/a^2 \approx 12.2$, confirmed that the reduction in amplitude of the primary roll pattern with Y at $X = \frac{1}{2}$ (as measured by $D_{1/2}$) is actually larger than that at $X = 0$ (as measured by D_0). The asymptotic solution of §4 suggests that this should be the case for values of a greater than about 0.8, although it was necessary to

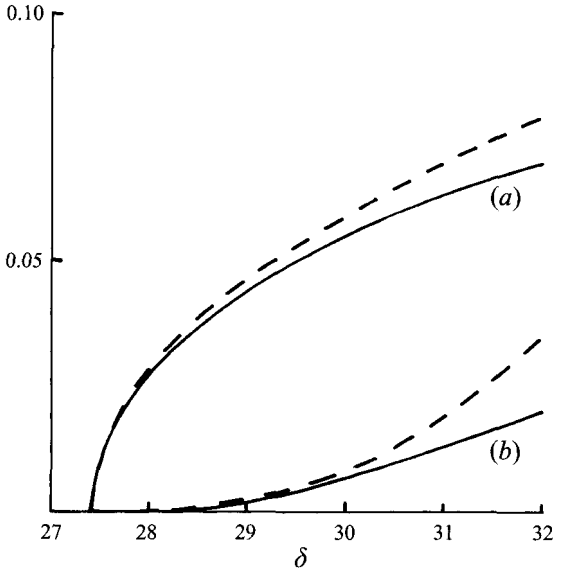

FIGURE 6. The computed and asymptotic solutions of figure 5 near the critial point $\delta = 27.4156$, shown by solid and dashed lines respectively. Note that here (b) shows $10D_{1/2}$.

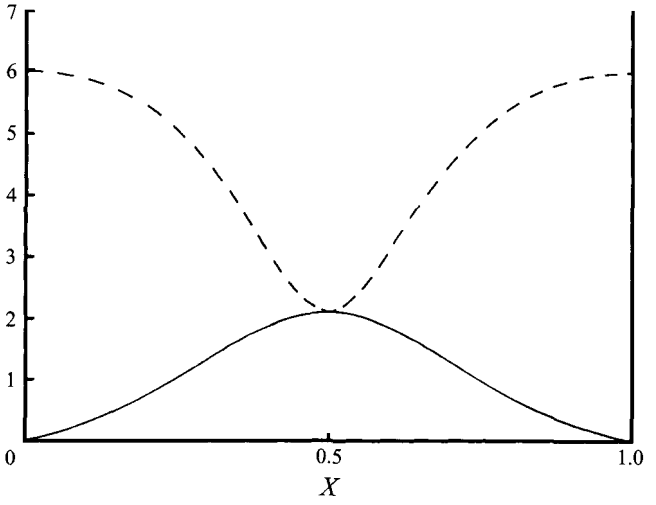

FIGURE 7. Steady-state profiles of A and B shown by solid and dashed lines respectively on the centreline $Y = 0.5$ for $\delta = 40$ and an aspect ratio $a = 1$.

take a value of δ quite close to the critical value (12.5, for example) in order to observe this behaviour. For $a = 0.96$, the transition lines are located further into the interior of the container than for $a = 0.6$, with $X_0 \approx 0.25$ for $\delta = 40$ and $X_0 \approx 0.2$ for $\delta = 100$. The special case of a square container is particularly interesting (see Edwards 1988) and here for $\delta = 40$ the initial distributions (6.1) evolved to a symmetric steady-state solution in which $A(X, Y) = B(Y, X)$, with a common value of about 2.15 at the centre of the container (see figure 7).

7. Discussion

A model of the interaction between orthogonal rolls has been used as a basis for describing patterns of convection in shallow rectangular containers. The initial onset of rolls parallel to the shorter lateral boundaries is confirmed, and then, at a second critical point, the emergence of perpendicular rolls close to these boundaries. These local cross-rolls influence the speed of the primary roll pattern in the central part of the container, causing a small reduction in amplitude in the middle portion of each roll. The nature of this variation is determined analytically for values of the control parameter close to the critical point and numerically in other cases. The results of this weakly nonlinear theory are in good agreement with the full numerical simulations of the model equation (2.1) by Greenside & Coughran (1984). They obtained steady-state results for two small values of ϵ, namely 0.03 and 0.1, with $L = 29.2\pi$ and $a = 0.667$. From (2.9), these cases are equivalent to $\delta = 63.11$ and $\delta = 210.4$ respectively. Computations for the present system with these parameter values were carried out and the values of X at which $A = (\delta - \pi^2/a^2)^{1/2}/\sqrt{2}$ on $Y = a/2$ used to estimate the location of the transition line, yielding $X = 0.17$ and $X = 0.15$ respectively. These correspond to values of x equal to 15.6 and 13.8, which compare well with the extent of the y-rolls shown in figure 9 of Greenside & Coughran (1984).

Experimental work in which detailed observations have been made of roll patterns in rectangular boxes includes that by Stork & Muller (1972) and Kirchartz & Oertel (1988). Gollub, McCarriar & Steinman (1982) used an automated laser-Doppler scanning technique to carry out an extensive study of pattern evolution in a large Rayleigh–Bénard cell with $a = 2/3$ whose ratio of the largest horizontal dimension to the fluid depth was 29.2. Many of the complex roll patterns observed in their experiments were also observed in a qualitative sense in the numerical simulations of Greenside & Coughran (1984), although most of the experiments were carried out at Rayleigh numbers two or more times the critical value, well beyond the small values of ϵ referred to above and the scope of the present theory. Further experimental work is needed to confirm the roll structures predicted in the slightly supercritical case. One feature of the numerical simulations and experiments at higher Rayleigh numbers is the occurrence of rolls at varying angles to the lateral boundaries. At slightly supercritical Rayleigh numbers the cross-roll instability suggests that an orthogonal pattern will be preferred and the present theory only incorporates rolls parallel and perpendicular to the lateral walls.

In the present paper attention has been focused on the regime equivalent to Rayleigh numbers order L^{-2} in excess of the critical value for an infinite layer, and also on the case where the lateral boundary conditions are null. Further work is needed to consider both lateral forcing at the boundaries and higher Rayleigh number regimes where phase winding effects may be significant. These have been considered in the case of purely two-dimensional rolls for the Rayleigh–Bénard problem with stress-free upper and lower surfaces by Cross *et al.* (1983), where it is found that the lateral boundaries play an important role in selecting the wavelength of the roll pattern in the main body of the container. It remains to be seen how the more complicated three-dimensional motion near the lateral walls identified here affects the wavelength selection mechanism and in what range of Rayleigh numbers phase winding effects become significant. This will require an investigation of the structure of the present solution as $\delta \to \infty$ and incorporation of fully complex amplitude functions A and B, along with a more detailed appraisal of the local structures around the lateral walls, in the corners and along the transition lines. Preliminary investigations suggest that the asymptotic

structure of the solution as $\delta \to \infty$ is quite complicated and it is expected that the boundary layers of thickness $X \sim \delta^{-1/2}$ which develop near the shorter lateral walls will have some features in common with the semi-infinite problem analysed by Daniels & Weinstein (1992). They showed that with $A = \lambda$ on $X = 0$ then in the limit as $\lambda \to 0$ the layer moves away from the wall, and so for the case $\lambda = 0$ it is interesting to conjecture how higher-order effects, perhaps associated with the residual Y-dependence of the solution as $\delta \to \infty$, may act to maintain a steady-state configuration and determine the location of the transition line as $\delta \to \infty$. It is hoped to report on this important limiting case in a future paper.

Support from the Science and Engineering Research Council in the form of a Visiting Fellowship Research Grant is gratefully acknowledged.

REFERENCES

ABRAMOWITZ, M. & STEGUN, I. A. 1965 *Handbook of Mathematical Functions*. Dover.

BROWN, S. N. & STEWARTSON, K. 1977 *Stud. Appl. Maths* **57**, 187.

CHEN, M. M. & WHITEHEAD, J. A. 1968 *J. Fluid Mech.* **31**, 1.

CROSS, M. C. 1980 *Phys. Fluids* **23**, 1727.

CROSS, M. C., DANIELS, P. G., HOHENBERG, P. C. & SIGGIA, E. D. 1983 *J. Fluid Mech.* **127**, 155.

DANIELS, P. G. 1977 *Proc. R. Soc. Lond.* A **358**, 173.

DANIELS, P. G. 1978 *Mathematika* **25**, 216.

DANIELS, P. G. & ONG, C. F. 1990 *J. Fluid Mech.* **215**, 503.

DANIELS, P. G. & WEINSTEIN, M. 1992 *Q. J. Mech. Appl. Maths* **45**, 315.

DAVIS, S. H. 1967 *J. Fluid Mech.* **30**, 465.

EDWARDS, B. F. 1988 *J. Fluid Mech.* **191**, 583.

GOLLUB, J. P., MCCARRIAR, A. R. & STEINMAN, J. F. 1982 *J. Fluid Mech.* **125**, 259.

GREENSIDE, H. S. & COUGHRAN, W. M. 1984 *Phys. Rev.* A **30**, 398.

KIRCHARTZ, K. R. & OERTEL, H. 1988 *J. Fluid Mech.* **192**, 249.

KOSCHMIEDER, E. L. 1993 *Benard Cells and Taylor Vortices*. Cambridge University Press.

NEWELL, A. C. & WHITEHEAD, J. A. 1969 *J. Fluid Mech.* **38**, 279.

POMEAU, Y. & MANNEVILLE, P. 1980 *Phys. Lett.* A **75**, 296.

POMEAU, Y. & ZALESKI, S. 1981 *J. Phys. Paris* **42**, 515.

SCHLUTER, A., LORTZ, D. & BUSSE, F. H. 1965 *J. Fluid Mech.* **23**, 129.

SEGEL, L. A. 1969 *J. Fluid Mech.* **38**, 203.

SIVAPRAGASAM, V. R. 1995 Finite amplitude patterns of convection near a lateral boundary. PhD thesis, City University, London.

STORK, K. & MULLER, U. 1972 *J. Fluid Mech.* **54**, 599.

SWIFT, J. B. & HOHENBERG, P. C. 1977 *Phys. Rev.* A **15**, 319.